



## PROCEEDING OPEN ACCESS

# Modeling the Emission and Polarization Properties of Pulsating Ultraluminous X-Ray Sources

S. Conforti<sup>1,2</sup>  | L. Zampieri<sup>1</sup> | R. Taverna<sup>2</sup> | R. Turolla<sup>2,3</sup> | N. Brice<sup>4</sup> | F. Pintore<sup>5</sup> | G. L. Israel<sup>6</sup> 

<sup>1</sup>INAF, Osservatorio Astronomico di Padova, Padova, Italy | <sup>2</sup>Università degli studi di Padova, Padova, Italy | <sup>3</sup>Mullard Space Science Laboratory, University College London, London, UK | <sup>4</sup>Centre for Astrophysics Research, University of Hertfordshire, Hatfield, UK | <sup>5</sup>INAF, IASF, Palermo, Italy | <sup>6</sup>INAF, Osservatorio Astronomico di Roma, Roma, Italy

**Correspondence:** S. Conforti ([silvia.conforti@studenti.unipd.it](mailto:silvia.conforti@studenti.unipd.it))

**Received:** 28 November 2024 | **Accepted:** 2 December 2024

**Funding:** Financial support from the INAF Research Grant “Uncovering the optical beat of the fastest magnetized neutron stars (FANS)” and Italian MUR through grant PRIN 2022LWPEXW.

**Keywords:** neutron stars | polarization | x-ray emission

## ABSTRACT

Pulsating Ultraluminous X-ray Sources (PULXs) are a class of extragalactic sources with high X-ray luminosity, in excess of  $10^{39}$  erg s<sup>-1</sup>, and showing pulsations that associate them with neutron stars accreting at a super-Eddington rate. A simplified model is presented, which describes the thermal emission from an accreting, highly magnetized neutron star and includes the contributions from an accretion disk and an accretion envelope surrounding the star magnetosphere. Through numerical calculations, we determine the flux, pulsed fractions, polarization degree, and polarization angle considering various viewing geometries. The model is confronted with the *XMM-Newton* spectra of M51 ULX-7, and the best fitting viewing geometries are estimated. A measurement of the polarization observables, which will be available with future facilities, along with spectroscopic data obtained with *XMM-Newton*, will provide considerable additional information on these sources.

## 1 | Introduction

Ultraluminous X-ray sources (ULXs) were first identified in external galaxies during the 1980s using the Einstein X-ray Observatory (Fabbiano 1989). These sources are characterized by an extremely high X-ray luminosity, up to  $L \sim 10^{41}$  ergs<sup>-1</sup>, which exceeds the Eddington limit for a solar-mass object (see e.g., Kaaret, Feng, and Roberts 2017, for a review). ULXs are characterized by a higher occurrence in star-forming galaxies (Swartz et al. 2004), a turnover in the 2–10 keV range, a softer component below 1 keV, and spectral variability over time (e.g., Gladstone, Roberts, and Done 2009; Pintore and Zampieri 2012).

The large amount of energy emitted and the X-ray variability led to believe that they are binary systems with a massive

donor transferring material onto a black hole (Kaaret, Feng, and Roberts 2017). Initially, ULXs were believed to be powered by intermediate-mass black holes (IMBHs) larger than  $100 M_{\odot}$  (Colbert and Mushotzky 1999), as the Eddington limit would then allow accretion at sub-Eddington rates. Later, super-Eddington accretion onto stellar-mass black holes ( $M_{BH} \sim 10 - 20 M_{\odot}$  (Feng and Soria 2011) and  $M_{BH} \sim 30 - 80 M_{\odot}$  (Zampieri and Roberts 2009)) was considered, but this required emission to be (slightly) beamed to match the observed luminosity (Poutanen et al. 2007).

In Bachetti et al. (2014), the discovery of pulsations in M82 X-2, an ULX in the M82 galaxy, led to believe that some ULXs could be powered by neutron stars (NS) (Bachetti et al. 2014). This discovery was followed by others (see, e.g., Quintin et al. 2021,

---

This is an open access article under the terms of the [Creative Commons Attribution](https://creativecommons.org/licenses/by/4.0/) License, which permits use, distribution and reproduction in any medium, provided the original work is properly cited.

© 2025 The Author(s). *Astronomische Nachrichten* published by Wiley-VCH GmbH.

and references there in), so populating the subclass of pulsating ULXs (PULXs).

However, explaining how neutron stars can emit at such levels remains challenging, given that the Eddington luminosity for a neutron star is  $\approx 10^{38}$  erg/s. Theoretical work on accretion onto highly magnetized NSs, starting with Basko and Sunyaev (1976), proposed that a strong magnetic field could play a role, particularly by reducing the opacity of photons polarized perpendicular to the magnetic field, thereby increasing the Eddington limit and allowing more radiation to escape (see Brice et al. 2021; Lyubarskii and Syunyaev 1988; Mushtukov et al. 2015).

We present here a simplified model (torusdisk hereafter) that reproduces the X-ray thermal emission of pulsating ULXs, in terms of emission from an accretion disk and an accretion envelope, which is modeled following the shape of the dipole magnetic field lines, that extend up to the magnetospheric radius. To this aim, we adapted the numerical code by Taverna et al. (2015), which calculates the flux of photons coming from the part in view of the system as a function of both the photon energy and the star rotational phase, so to compute spectra and light curves of PULXs in different energy bands. In addition to the flux, the code also computes the polarization degree (PD) and polarization angle (PA), again as a function of energy and phase. We compared the simulations with the observational data of two PULXs, to test if the model can reproduce the properties exhibited by real sources. Here we focus on one of the two: M51 ULX-7 (aka NGC 5194 X-7), located in the outskirts of a young open cluster in a spiral arm of its host galaxy. It is a high-mass X-ray binary (HMXB) with a O-B companion with mass  $\gtrsim 8 M_{\odot}$  (Rodríguez Castillo et al. 2020) and exhibits an X-ray luminosity of  $6 \times 10^{39}$  erg s $^{-1}$ . The main goal of this work is to derive information on the viewing geometry of this source and its thermal and polarization properties. We use polarization to help discriminating among different viewing geometries in case spectral results are degenerate. Indeed, polarimetric measurements could be a powerful tool for the study of highly magnetized neutron stars in PULXs. While PULXs are too weak for present polarimetric missions, in particular for the Imaging X-ray Polarimetry Explorer (IXPE, Weisskopf et al. (2022)), observations with future more sensitive facilities, along with spectroscopic data, will provide considerable additional information on these sources.

## 2 | Physical Model

The model simulates emission from an accreting magnetized neutron star (NS) in a binary system, where the accreting material flows from the donor star through a geometrically thin accretion disk. At the Alfvén radius ( $r_A$ ), where the magnetic pressure equals the ram pressure of the gas, matter is channeled along the magnetic field lines toward the NS poles, forming a structure referred to as a “torus” (see Figure 1; Brice et al. 2023). This torus is optically thick at high accretion rates typical of PULXs. The NS is assumed to have a mass of  $1.4 M_{\odot}$ , a radius of 10 km, and a dipolar magnetic field with a polar strength of  $10^{12} - 10^{13}$  G. The magnetic field lines are described by the following equation for a dipole magnetic field:

$$r = R_{\max} \sin^2 \theta, \quad (1)$$

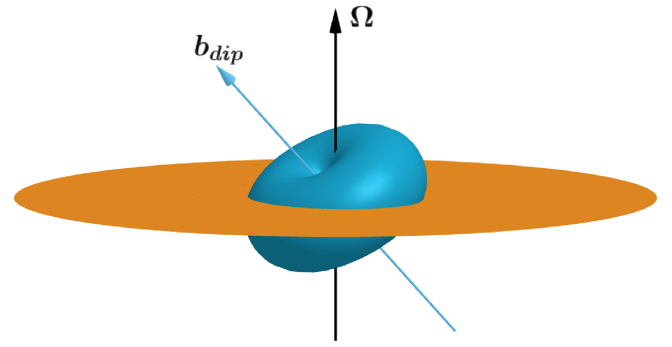


**FIGURE 1** | A 3D representation of the source geometry. The torus is in blue, while the disk is in orange. The magnetic axis  $\mathbf{b}_{\text{dip}}$ , and the spin axis  $\Omega$  are also shown.

where  $\theta$  is the magnetic colatitude, and  $R_{\max} = r_A$  in this case. We assume that both the disk and torus are in Local Thermal Equilibrium (LTE). The disk temperature follows the thin-disk profile (Shakura and Sunyaev 1973):

$$T(r) = T_{\text{in}} \left( \frac{R_{\text{in}}}{r} \right)^{3/4}, \quad (2)$$

where  $T_{\text{in}}$  is the temperature at the inner disk radius  $R_{\text{in}}$ , which coincides with the intersection of the torus and disk, so at  $r = R_{\max}$ . The torus temperature varies with the magnetic colatitude and is given by (Brice et al. 2023):

$$T_{\text{out}} = T_{\text{in}} \tau^{-1/4}, \quad (3)$$

where  $T_{\text{out}}$  ( $T_{\text{in}}$ ) is the temperature at the outer (inner) boundary of the torus, and  $\tau$  is the optical depth. The latter in turn depends on the magnetic colatitude  $\theta$ . The fact that the optical depth varies within the torus leads to a multicolor blackbody spectrum.

### 2.1 | Polarization

Radiation emitted by strongly magnetized neutron stars is expected to be highly polarized in two normal modes, the ordinary (O) and extraordinary (X) ones (e.g., Lai et al. 2010). The O-mode has an electric field oscillating in the plane of the propagation vector  $\mathbf{k}$  and the local magnetic field  $\mathbf{B}$ , while in the X-mode it oscillates perpendicularly to both vectors. The cross-sections for X-mode photons are significantly reduced below the electron cyclotron energy,  $E_{\text{c,e}} \approx 11.6 (B/10^{12} \text{ G}) \text{ keV}$ , by a factor of  $\sim (B/B_Q)^2$ , making the medium optically thin for X photons, which helps explaining the super-Eddington luminosity in X-rays.

Strong magnetic fields also modify the optical properties of the vacuum, particularly through vacuum birefringence (Heisenberg and Euler 1936), which affects photons propagating in a strongly magnetized vacuum. This forces polarization modes to remain unchanged within a region close to the star surface where the magnetic field is strong enough. Inside this region, the photon’s electric field vector adapts instantaneously to the local magnetic field direction, while outside (and farther from the star) the direction of the electric field vector becomes frozen. The boundary between these regions is called adiabatic radius (Taverna et al. 2015):

$$\frac{r_{\text{pl}}}{R_{\text{NS}}} \sim 5 \left( \frac{E}{1 \text{ keV}} \right)^{1/5} \left( \frac{R_{\text{NS}}}{10 \text{ km}} \right)^{1/5} \left( \frac{B_p}{10^{11} \text{ G}} \right)^{2/5}, \quad (4)$$

where  $E$  is the photon energy,  $B_p$  the polar magnetic field strength, and  $R_{\text{NS}}$  the NS radius.

For the magnetic field strength ( $\sim 10^{13}$  G) and photon energies considered here (0.1–1 keV), the Alfvén radius is much larger than the adiabatic radius ( $R_{\text{max}} \sim 50R_{\text{NS}}$ , while  $r_A \sim 36R_{\text{NS}}$ ), so a large part of the torus lies outside the adiabatic region. Therefore, we assume that radiation from this region is unpolarized, while radiation from regions close to the magnetic poles (inside  $r_{\text{pl}}$ ) has a non-zero intrinsic polarization degree,

$$\Pi_L = \left| \frac{N_X - N_O}{N_X + N_O} \right|, \quad (5)$$

where  $N_X$  ( $N_O$ ) is the number of X (O) photons. Radiation from the disk is assumed to have negligible polarization since it originates outside  $r_{\text{pl}}$ , where  $B$  is quite small.

For both O and X photons, the polarization degree (PD) and polarization angle (PA) are expressed in terms of the (normalized) Stokes parameters  $I$ ,  $Q$ , and  $U$  (Rybicki and Lightman 1991). In a reference frame with the  $z$  axis along the wave unit vector  $\vec{k}$ , and the  $y$  axis in the  $(\vec{k}, \vec{B})$  plane, the parameters for the emitted X and O photons are:  $(I, Q, U)_X = (1, 1, 0)$ , and  $(I, Q, U)_O = (1, -1, 0)$ ; The last Stokes parameter,  $V$ , describing circular polarization, is not considered here. The polarization observables are calculated by summing the Stokes parameters of each emitting photon in a fixed reference frame, which we choose to be that of the polarimeter (see Taverna et al. 2015), taking into account that each photon’s reference frame is rotated by an angle  $\alpha_i$  with respect to the polarimeter frame. Once we have the final Stokes parameters the observed PD and PA are given by (Rybicki and Lightman 1991):

$$\text{PD} = \frac{\sqrt{Q^2 + U^2}}{I}, \quad \text{PA} = \frac{1}{2} \arctan\left(\frac{U}{Q}\right), \quad (6)$$

where the Stokes parameters  $Q$  and  $U$  refer to the total radiation, that is, the sum of the  $Q_i$  and  $U_i$  of the collected photons. The polarization degree measured at infinity is generally lower than at emission due to the geometrical factors  $\sin(2\alpha_i)$  and  $\cos(2\alpha_i)$ , which appear in the expressions for  $Q_i$  and  $U_i$ . If the magnetic field topology is tangled,  $\alpha_i$  spans the entire  $0-2\pi$  range, increasing depolarization. In contrast, in a more uniform magnetic field (like at  $r_{\text{pl}}$ ), the angles are more similar, reducing depolarization. Thus, when vacuum birefringence is accounted for and Stokes parameters are computed at  $r_{\text{pl}}$ , the polarization pattern at the surface is likely preserved at the observer.

## 2.2 | Numerical Implementation

To compute the spectral and polarization properties of the emitted radiation, we used the ray-tracer code presented in Taverna et al. (2015),<sup>1</sup> but adapted to our model, in particular to a different emitting surface (torus and disk). The code starts by computing the visible part of the source assuming a specific viewing geometry, that is given by two angles:  $\chi$ , between the LOS and the spin axis of the star, and  $\xi$ , between the magnetic axis of the star and

its spin axis. We consider the source surface, comprising the disk and the torus, as a collection of small emitting patches. The grid is made by 50 bins in  $\theta$ ,  $\phi$  (longitude), and  $r$  (radial distance), while for both the energy and rotational phase we take 30 bins. The phase is measured from the projection of the LOS onto the plane perpendicular to the spin axis.

Each point in view emits as a blackbody with a temperature computed from Equation (2), if the point is on the disk, or from Equation (3), if the point is on the torus. The result is a matrix with the emitted intensity as function of both the phase and the energy. Summing over the phase we obtain the spectrum, while summing over the energy we obtain the light curves. Similarly, we do for the Stokes parameters.

## 3 | Data Reduction

We analyzed a sample of *XMM-Newton* and *NuSTAR* observations of M51 ULX-7, one of the two PULXs taken as benchmarks for our study.

We made use of three *XMM-Newton* observations for M51 ULX-7 (Obs. ID: 0824450901, 0830191501 and 0830191601), carried out between 2018 May and June. We extracted EPIC-pn data using the SAS v.14.0. package.<sup>2</sup> Spectra were obtained by selecting events with the PATTERN  $\leq 4$  for EPIC-pn (single- and double-pixel events) and setting “FLAG = 0” to ignore bad pixels and events coming from the CCD edges. Epochs of high background were also removed from the analysis. Source and background events were extracted from circular regions with radius 30” and 60”, respectively. The spectra were rebinned in order to have at least 25 counts per energy bin.

## 4 | Results

We started by comparing the light curves of the *XMM-Newton* observations with the simulated ones to constrain the geometry of view, which significantly affects the flux modulation. In particular, we compared the observed and simulated pulsed fractions (PFs), defined as  $\text{PF} = (\max(\text{Flux}) - \min(\text{Flux})) / (\max(\text{Flux}) + \min(\text{Flux}))$ . After constraining the viewing geometry, we compared the spectra determining the temperature at the inner radius of the accretion disc ( $T_{\text{in}}$ ). For the comparison of the pulse profiles, we considered six possible viewing geometries while, for the comparison of the spectra, we choose 16 values of  $T_{\text{in}}$ , selected on the basis of values found in the literature. We then analyzed the polarization degree and polarization angle for each source using the best fit viewing geometry and  $T_{\text{in}}$ .

### 4.1 | Comparison of the Light Curves

We made a direct comparison of the light curves considering the 2–3 keV and 3–4 keV energy bands, since we expect that at these energies the torusdisk model (in particular the emission of the torus) dominates. We compared each observed profile with six simulations having different geometries of view, each differing only for the angle  $\chi$  (ranging from  $10^\circ$  to  $60^\circ$ ). The value of  $\xi$

was fixed at  $10^\circ$  to represent a general non-aligned magnetic rotator case, and angles beyond  $60^\circ$  were not considered, because we noted in the simulations that the PF decreases if  $\chi > 60^\circ$ .

To perform simulations we fixed some input parameters: the magnetic field strength  $B$ , the magnetospheric radius  $R_{\max}$ , the torus temperature, and the disk radius  $R_{\text{disk}}$ . M51 ULX-7 has a surface magnetic field strength between  $8 \times 10^{11}$  G and  $10^{13}$  G (Rodríguez Castillo et al. 2020), so we set a lower and upper limit,  $B = 10^{12}$  G and  $B = 8 \times 10^{12}$  G, respectively. The magnetospheric radius ( $R_{\max}$ ) and torus temperature were computed according to  $B$ . The disk outer radius was set to  $200R_{\text{NS}}$ , as beyond this radius the emitted flux falls below 0.1 keV, outside the range considered here.

We determined the following boundaries for the geometry of view, the lower limit being  $\chi = 20^\circ, \xi = 10^\circ$  and the upper limit  $\chi = 60^\circ, \xi = 10^\circ$  (Figure 2). For these geometries, the observed PFs across different energy bands show general agreement with the simulated PFs.

## 4.2 | Comparison of the Spectra

We constrained  $T_{\text{in}}$  by comparing the spectra with both the viewing geometries  $\chi = 20^\circ, \xi = 10^\circ$  and  $\chi = 60^\circ, \xi = 10^\circ$ . Simulations

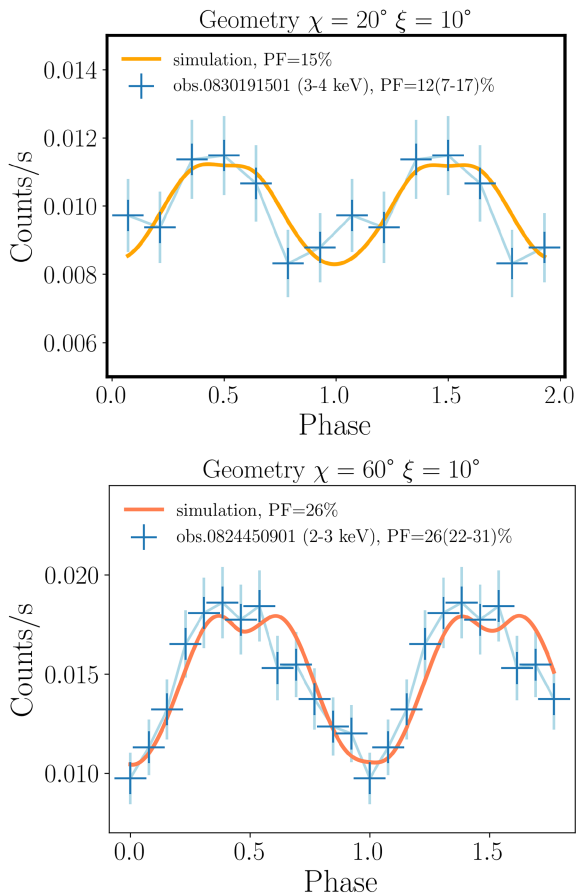


**FIGURE 2** | Light curve comparisons for M51 ULX-7. On the left we compare the pulsed profile with the geometry of view lower limit (in yellow), on the right the pulsed profile confronted with the geometry of view upper limit (in orange).

were performed with  $T_{\text{in}}$  ranging from 0.25 to 0.5 keV in 16 bins, and fixing the magnetic field strength. The spectrum was fitted with a multicomponent model: a phenomenological soft blackbody, our model spectrum for the torus and disk emission, and a phenomenological high-energy power-law component. The soft blackbody component represents emission from radiative winds originating from the accretion disk at super-Eddington rates, while the high energy cutoff power-law the non-thermal emission from an accretion column. Both models are taken from XSPEC (Arnaud 1996). The total spectrum is corrected for absorption with the WABS model of XSPEC (Morrison and McCammon 1983). The spectra are well reproduced by the model, with a fitted value  $T_{\text{in}}$  of 0.3 keV, and a fixed value of  $B = 8 \times 10^{12}$  G, for both the viewing geometries (see Figure 3), consistent with previous studies (Brightman et al. 2022; Rodríguez Castillo et al. 2020).

## 4.3 | Polarization

We simulated the polarization properties considering a magnetic field strength of  $8 \times 10^{12}$  G. We analyzed how polarization degree (PD) and polarization angle (PA) vary with energy, phase, and viewing geometry for different intrinsic polarization fractions,  $\Pi_{\text{L}}$ .

In simulating the polarization properties, we considered a field with strength of  $8 \times 10^{12}$  G at the poles. For photons escaping from the adiabatic region we fixed the intrinsic polarization fraction,  $\Pi_{\text{L}}$ , at 60% in the X-mode. This value was not computed self-consistently since this would have required to solve the full radiation transport problem, which is definitely outside the scope of the present work. Nevertheless, in the presence of strong magnetic fields ( $\gtrsim 10^{13}$  G) X-mode photons are expected to dominate the emission, so our assumption is not unreasonable. In our analyzes, we also varied  $\Pi_{\text{L}}$  fixing the geometry of view at  $\chi = 60^\circ, \xi = 10^\circ$ .

We show in Figure 4 the energy- and phase-dependent PD, and PA, for two different geometries of view,  $\chi = 60^\circ, \xi = 10^\circ$  and  $\chi = 20^\circ, \xi = 10^\circ$ . In each panel, the polarization degree increases

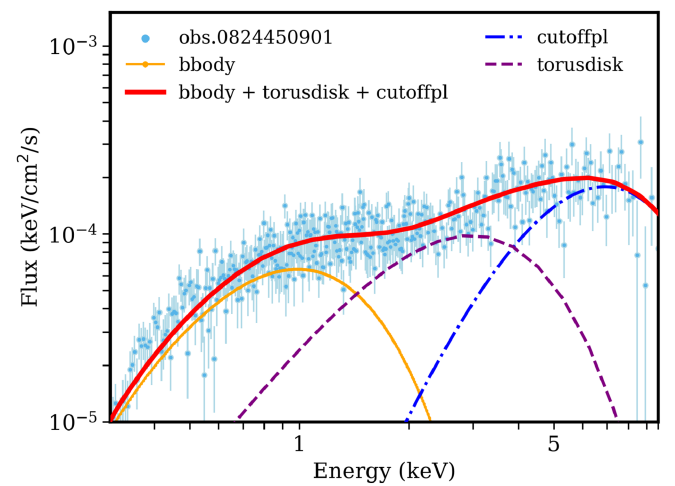


**FIGURE 3** | Spectrum of M51 ULX-7 fitted with a multicomponent model consisting of a soft blackbody (orange), our torus/disk model (purple), and a high energy cutoff power-law (blue).



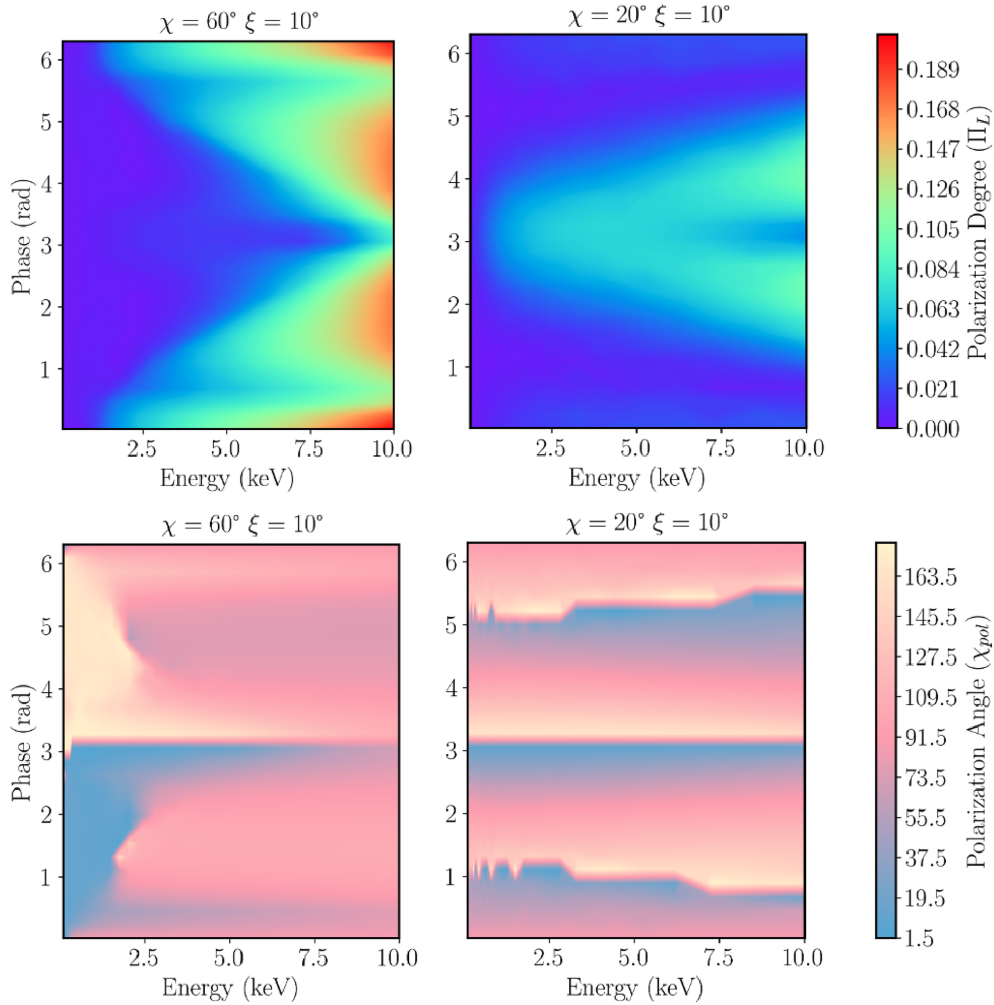


**FIGURE 4** | PD and PA variation with energy and phase for different geometries of view, a magnetic field  $B = 8 \times 10^{12}$  G, and an intrinsic polarization fraction  $\Pi_L = 60\%$ .

with the energy and shows an oscillating behavior with the phase, that changes going from  $\chi = 20^\circ$  to  $\chi = 60^\circ$ . The former is a consequence of the strong magnetic field considered in the model and the latter is, instead, a consequence of the rotation of the source combined with the geometry of view.

Results show that a variation in the intrinsic polarization degree only leads to an overall variation in the value of the PD, without changing its behavior with energy and phase. This reinforces the hypothesis that, even if the intrinsic polarization value assumed in the model may be different from the one computed self-consistently, we can still distinguish the geometry of view through the energy and phase variations of PD, since they do not depend on the value of  $\Pi_L$ , but only on the geometry of view and magnetic field of the source.

## 5 | Conclusions

The aim of this paper is to constrain the geometry of view, the magnetic field strength and thermal properties of pulsating ULXs, reproducing the thermal radiation emitted by a highly magnetized neutron star accreting at a super-Eddington rate,

considering the emission from an accretion disk and an optically thick envelope surrounding the magnetosphere. The model reproduces the light curves, and the spectra of PULXs, with the addition of two phenomenological components: a soft blackbody component and a high energy cut-off power law. Besides the spectral properties, we also incorporated the polarization observables of the emitted radiation, focusing our analyses on the polarization degree.

We used and modified the ray-tracer code presented in Taverna et al. (2015), to reproduce spectra and light curves of PULXs in two different energy bands. The model also simulates the polarization degree and angle of the radiation emitted as a function of energy and phase. We tested the model on M51 ULX-7 using *XMM-Newton* observations. The aim was to test the validity of our model and derive information on the geometry of view, magnetic field, thermal and polarization properties of PULXs.

In the model, we considered the emission from a highly magnetized neutron star in an accreting binary system with a mass of  $1.4 M_\odot$ , radius 10 km, and magnetic field strength within  $10^{12}$  and  $\sim 10^{13}$  G. The accreting material originates from the donor star and proceeds through a geometrically thin accretion disk

up to the Alfvén radius, where particles are funneled along the magnetic field lines, which follow a dipole field topology, toward the magnetic poles of the star. Each point of the torus and the disk emits like a blackbody, with a local temperature calculated with Equations (2) and (3). The emission of the whole source is then a complex, multicolor blackbody. We considered as well polarization observables, taking as polarized only the radiation coming from below the adiabatic radius  $r_{\text{pl}}$ . We computed the flux and the polarization observables for different viewing geometries ( $\chi$ ,  $\xi$ ) of each source.

We made direct comparisons of the light curves considering the energy bands 2–3 keV and 3–4 keV. We compared each observed profile with six simulations having different geometries of view, and from these comparison we constrained the viewing geometry obtaining a lower and upper limit of the angle  $\chi$ , using them in the spectral analysis.

We compared spectra from different observations with those simulated by the model, selecting the best temperature at the inner radius of the disk,  $T_{\text{in}}$ , and obtaining an estimate of the strength of the magnetic field strength. For M51 ULX-7, assuming a magnetic field strength of  $8 \times 10^{12}$  G, we compared the spectrum with a multicomponent model that combines a soft blackbody, the torusdisk component, and a high energy cut-off power law. The best fitting internal disk temperature turned out to be  $T_{\text{in}} \approx 0.3$  keV. For a given viewing geometry, the polarization degree increases with the energy and shows an oscillating behavior with the phase. The former is a consequence of the strong magnetic field considered in the model, while the oscillating behavior with the phase is a consequence of the rotation of the source combined with the geometry of view. Fixing energy and phase but varying the angle  $\chi$ , we note that the value of the polarization degree increases. The variation of PD from one geometry of view to another could allow us to distinguish them, if observed polarization measurements are available.

The model reproduces well the observed spectrum of M51 ULX-7, particularly in the 1.5–5 keV interval, where the contribution of the torus with the disk is dominant.

## Acknowledgments

The work of SC was partially supported by the INAF Doctorate program. SC and LZ acknowledge financial support from the INAF Research Grant “Uncovering the optical beat of the fastest magnetized neutron stars (FANS)”. RTa and RTu acknowledge financial support from the Italian MUR through grant PRIN 2022LWPEXW. Open access publishing facilitated by Università degli Studi di Padova, as part of the Wiley-CRUI-CARE agreement.

## Conflicts of Interest

The authors declare no conflicts of interest.

## Endnotes

<sup>1</sup> This Ray-tracer code computes the polarization observables for a NS with a weak magnetic field, and with the sole torus as emitting component. Effects of strong gravity on photon propagation and on the stellar magnetic field are also taken into account.

<sup>2</sup> Spectra reduced with this version were already available in our archives. Since they are of enough high quality for the aims of this work and since

we do not expect significant differences, we choose not to reprocess the data with the latest SAS v21.0.0.

## References

- Arnaud, K. 1996. “Astronomical Data Analysis Software and Systems V.” In *ASP Conf.*, vol. 17.
- Bachetti, M., F. A. Harrison, D. J. Walton, et al. 2014. “An Ultraluminous X-Ray Source Powered by an Accreting Neutron Star.” *Nature* 514, no. 7521: 202–204.
- Basko, M., and R. A. Sunyaev. 1976. “The Limiting Luminosity of Accreting Neutron Stars With Magnetic Fields.” *Monthly Notices of the Royal Astronomical Society* 175, no. 2: 395–417.
- Brice, N., S. Zane, R. Turolla, and K. Wu. 2021. “Super-Eddington Emission from Accreting, Highly Magnetized Neutron Stars With a Multipolar Magnetic Field.” *Monthly Notices of the Royal Astronomical Society* 504, no. 1: 701–715.
- Brice, N., S. Zane, R. Taverna, R. Turolla, and K. Wu. 2023. “Observational Properties of Accreting Neutron Stars With an Optically Thick Envelope.” *Monthly Notices of the Royal Astronomical Society* 525, no. 3: 4176–4185.
- Brightman, M., M. Bachetti, H. Earnshaw, et al. 2022. “Evolution of the Spin, Spectrum and Superorbital Period of the Ultraluminous X-Ray Pulsar M51 ULX7.” *Astrophysical Journal* 925, no. 1: 18.
- Colbert, E. J., and R. F. Mushotzky. 1999. “The Nature of Accreting Black Holes in Nearby Galaxy Nuclei.” *Astrophysical Journal* 519, no. 1: 89.
- Fabbiano, G. 1989. “Populations of X-Ray Sources in Galaxies.” *Annual Review of Astronomy and Astrophysics* 27, no. 1: 87–138.
- Feng, H., and R. Soria. 2011. “Ultraluminous X-ray sources in the Chandra and XMM-Newton era.” *New Astronomy Reviews* 55, no. 5-6: 166–183.
- Gladstone, J. C., T. P. Roberts, and C. Done. 2009. “The Ultraluminous State.” *Monthly Notices of the Royal Astronomical Society* 397, no. 4: 1836–1851.
- Heisenberg, W., and H. Euler. 1936. “Folgerungen aus der Diracschen Theorie des Positrons.” *Zeitschrift für Physik* 98, no. 11-12: 714–732.
- Kaaret, P., H. Feng, and T. P. Roberts. 2017. “Ultraluminous X-Ray Sources.” *Annual Review of Astronomy and Astrophysics* 55: 303–341.
- Lai, D., W. Ho, M. van Adelsberg, C. Wang, and J. Heyl. 2010. “Polarized X-Rays From Magnetized Neutron Stars.” *X-ray Polarimetry: A New Window in Astrophysics* 157.
- Lyubarskii, Y. E., and R. Syunyaev. 1988. “Accretion Column Structure.” *Soviet Astronomy Letters* 14: 390.
- Morrison, R., and D. McCammon. 1983. “Interstellar Photoelectric Absorption Cross Sections, 0.03-10 keV.” *Astrophysical Journal, Part 1* 270: 119–122.
- Mushtukov, A. A., V. F. Suleimanov, S. S. Tsygankov, and J. Poutanen. 2015. “On the Maximum Accretion Luminosity of Magnetized Neutron Stars: Connecting X-Ray Pulsars and Ultraluminous X-Ray Sources.” *Monthly Notices of the Royal Astronomical Society* 454, no. 3: 2539–2548.
- Pintore, F., and L. Zampieri. 2012. “X-Ray Spectral States and Metallicity in the Ultraluminous X-Ray Sources NGC 1313 X-1 and X-2.” *Monthly Notices of the Royal Astronomical Society* 420, no. 2: 1107–1114.
- Poutanen, J., G. Lipunova, S. Fabrika, A. G. Butkevich, and P. Abolmasov. 2007. “Supercritically Accreting Stellar Mass Black Holes as Ultraluminous X-Ray Sources.” *Monthly Notices of the Royal Astronomical Society* 377, no. 3: 1187–1194.
- Quintin, E., N. A. Webb, A. Gúrpide, M. Bachetti, and F. Fürst. 2021. “A New Candidate Pulsating ULX in NGC 7793.” *Monthly Notices of the Royal Astronomical Society* 503, no. 4: 5485–5494.

- Rodríguez Castillo, G., G. L. Israel, A. Belfiore, et al. 2020. “Discovery of a 2.8 s Pulsar in a 2 Day Orbit High-Mass X-Ray Binary Powering the Ultraluminous X-Ray Source ULX-7 in M51.” *Astrophysical Journal* 895, no. 1: 60.
- Rybicki, G. B., and A. P. Lightman. 1991. *Radiative Processes in Astrophysics*. John Wiley & Sons.
- Shakura, N. I., and R. A. Sunyaev. 1973. “Black Holes in Binary Systems. Observational Appearance.” *Astronomy and Astrophysics* 24: 337–355.
- Swartz, D. A., K. K. Ghosh, A. F. Tennant, and K. Wu. 2004. “The Ultraluminous X-Ray Source Population from the *Chandra* Archive of Galaxies.” *Astrophysical Journal Supplement Series* 154, no. 2: 519.
- Taverna, R., R. Turolla, D. Gonzalez Caniulef, S. Zane, F. Muleri, and P. Soffitta. 2015. “Polarization of Neutron Star Surface Emission: A Systematic Analysis.” *Monthly Notices of the Royal Astronomical Society* 454, no. 3: 3254–3266.
- Weisskopf, M. C., P. Soffitta, L. Baldini, et al. 2022. “Imaging X-Ray Polarimetry Explorer: Prelaunch.” *Journal of Astronomical Telescopes, Instruments, and Systems* 8, no. 2: 26002.
- Zampieri, L., and T. Roberts. 2009. “Low-Metallicity Natal Environments and Black Hole Masses in Ultraluminous X-Ray Sources.” *Monthly Notices of The Royal Astronomical Society* 400, no. 2: 677–686.